Genetic Algorithm based Optimal Sensor Placement for L_1-regularized Damage Detection

Rongrong Hou[1], Yong Xia[1*], Qi Xia[1] and Xiaoqing Zhou[2]

[1]*Department of Civil and Environmental Engineering, The Hong Kong Polytechnic University, Kowloon, Hong Kong, China*

[2]*College of Civil Engineering, Shenzhen University, China*

*Corresponding author, email: ceyxia@polyu.edu.hk

Abstract

Sparse recovery theory has been applied to damage detection by utilizing the sparsity feature of structural damage. The theory requires that the columns of the sensing matrix suffices certain independence criteria. In l_1-regularized damage detection, the sensitivity matrix serves as the sensing matrix and is directly related to sensor locations. An optimal sensor placement technique is proposed such that the resulting sensitivity matrix is of the maximum independence in the columns or is of the least mutual coherence. Given a total number of sensors, the selection of sensor locations is a combinatorial problem. A genetic algorithm is thus used to solve this optimization problem, in which the mutual coherence of the sensitivity matrix is minimized. The obtained optimal sensor locations and associated sensitivity matrix are used in l_1-regularized damage detection. An experimental cantilever beam and a three-storey frame are utilized to verify the effectiveness and reliability of the proposed sensor

placement technique. Results show that using the modal data based on the optimal sensor placement can identify damage location and severity more accurately than using the ones based on uniformly selected sensor locations.

Keywords

Damage detection, Sensor placement, Genetic algorithm, Mutual coherence, l_1 regularization

1. Introduction

Structural damage detection based on vibration characteristics is receiving considerable attention over the past decades because of its efficiency in practice and simplicity of implementation [1-3]. Salawu [4] reviewed damage detection methods using frequency data. Doebling et al. [5] and Sohn et al. [6] conducted a comprehensive review of vibration-based damage detection methods and their applications to various types of structures. In most studies, natural frequencies and mode shapes are combined because natural frequencies can be measured accurately and mode shapes are sensitive to local damage.

The vibration-based damage detection is essentially an inverse problem and typically ill-posed. The sensitivity-based model updating is underdetermined because the number of identifiable modal parameters is usually smaller than that of unknown parameters. Therefore, regularization techniques have been used to obtain a unique and stable identification result [7]. On the other hand, structural damage usually appears in a few sections or members only, which is sparse compared with the large number of elements of the entire structure. According to sparse recovery theory, the l_1 regularization technique is particularly effective in recovering sparse vectors. For this reason, several investigators have used the l_1 regularization technique for structural

damage detection [8-10]. Compared with the conventional l_2 regularization technique, the l_1 regularization technique improves damage identification accuracy significantly with a few measurement data only [11-13].

In sparse recovery problems, the sensing matrix projects the unknown vector into a low-dimensional measurement vector. Recovery accuracy largely depends on the number of measurements and their degree of independence. The sensing matrix should be designed and optimized on the basis of some criteria to ensure the stable and exact recovery of the sparse vector [14, 15]. For example, the sensing matrix in signal processing and image reconstruction should suffice the restricted isometry property (RIP) [16, 17]. In structural damage detection, however, the sensing matrix has not been investigated. In l_1-regularized damage detection, the sensitivity matrix actually acts as the sensing matrix, and it is directly related to the mode shapes used or sensor locations. Different sensor locations result in different sensitivity matrices and consequently may affect damage identification results. In addition, the number of available sensors is always limited due to the economy and technology considerations in practice. Therefore, given a total number of sensors, selection of sensor locations is important such that the resulting modal data contain considerable features of the structure and structural damage can be detected accurately.

A number of techniques have been developed in recent years to determine the optimal sensor placement (OSP). However, most of these techniques aim to achieve the optimal qualities of modal properties [18-24]. OSP methods for damage detection are limited. For example, Hemez and Farhat [25] extended the effective independence concept and proposed the OSP technique for damage detection according to the strain energy distribution of the structure. Zhou *et al.* [26] introduced a new sensor placement index in terms of the ratio of two parameters, namely, the contribution of the measurement points to the Fisher information matrix [27], and the damage sensitivity to the measurement noise [28].

Sensor placement is a typical combinatorial problem, and the global optimum is difficult to obtain using conventional techniques. With the development of computational intelligence, various algorithms have been widely used for damage detection and structural health monitoring [29, 30]. Among them, genetic algorithms (GAs) have been widely used and proved to be effective in solving combinatorial optimization problems [31]. Yao [32] perhaps was the first to use a GA to optimize sensor placement for modal identification, in which the determinant of the Fisher information matrix was selected as the fitness function. Worden and Burrows [33] applied a GA to determine the sensor distribution for fault diagnosis. Liu *et al.* [34] introduced an improved GA to find the OSP for spatial lattice structures, in which modal strain energy and modal assurance criteria were taken as fitness functions.

In this study, a GA-based OSP technique is developed for l_1-regularized damage identification. As described previously, the columns of the sensitivity matrix should be as independently as possible to achieve an accurate damage identification result. Therefore, the OSP is obtained such that the mutual coherence of the sensitivity matrix is as small as possible. A laboratory-tested cantilever beam and a three-storey frame are used to demonstrate the feasibility of the proposed method.

2. L_1-regularized Damage Detection

In sensitivity-based model updating, the relationship between changes in modal parameters $\{\Delta R\}$ and damage parameters $\{p\}$ can be linearly expressed as [11]

$$[\mathrm{S}]\{p\} = \{\Delta R\} = \{R^E\} - \{R^0\}, \tag{1}$$

where $\{R^E\}$ and $\{R^0\}$ refer to the measured and initial analytical modal parameters, respectively; and $[\mathrm{S}]$ is the sensitivity matrix which is defined as the derivative of the modal parameters with respect to the damage parameters. In this study, natural frequencies and mode shapes are utilized in the model updating. Therefore, the

sensitivity matrix consists of the corresponding two parts as

$$[\mathrm{S}] = \begin{bmatrix} \mathrm{S}_\lambda \\ \mathrm{S}_\phi \end{bmatrix} \tag{2}$$

where $[\mathrm{S}_\lambda]$ and $[\mathrm{S}_\phi]$ are the sensitivity matrices of eigenvalues $\{\lambda\}$ and eigenvectors $\{\phi\}$ with respect to $\{p\}$, respectively. $[\mathrm{S}_\lambda]$ can be expressed as

$$[\mathrm{S}_\lambda] = \left[\mathrm{S}_{\lambda_1}, \mathrm{S}_{\lambda_2}, \cdots, \mathrm{S}_{\lambda_m}\right]^T \tag{3a}$$

$$\{\mathrm{S}_{\lambda_i}\} = \frac{\partial \lambda_i}{\partial \{p\}} = \left\{\frac{\partial \lambda_i}{\partial p_1}, \frac{\partial \lambda_i}{\partial p_2}, \cdots, \frac{\partial \lambda_i}{\partial p_n}\right\} \tag{3b}$$

where $\{\lambda_i\}$ is the *i*th eigenvalue $(i = 1,2, \cdots m)$, m is the number of available modes in the model updating, and n is the number of elements in the finite element (FE) model. The eigenvector sensitivity matrix $[\mathrm{S}_\phi]$ can be expressed as

$$[\mathrm{S}_\phi] = \left[\mathrm{S}_{\phi_1}, \mathrm{S}_{\phi_2}, \cdots, \mathrm{S}_{\phi_m}\right]^T \tag{4a}$$

$$[\mathrm{S}_{\phi_i}] = \frac{\partial \{\phi\}_i}{\partial \{p\}} = \begin{bmatrix} \frac{\partial \phi_{1,i}}{\partial p_1} & \frac{\partial \phi_{1,i}}{\partial p_2} & \cdots & \frac{\partial \phi_{1,i}}{\partial p_n} \\ \frac{\partial \phi_{2,i}}{\partial p_1} & \frac{\partial \phi_{2,i}}{\partial p_2} & \cdots & \frac{\partial \phi_{2,i}}{\partial p_n} \\ \vdots & \vdots & \ddots & \vdots \\ \frac{\partial \phi_{np,i}}{\partial p_1} & \frac{\partial \phi_{np,i}}{\partial p_2} & \cdots & \frac{\partial \phi_{np,i}}{\partial p_n} \end{bmatrix} \tag{4b}$$

where $\{\phi_{j,i}\}$ is the *i*th mode shape at the *j*th point $(j = 1,2, \cdots np)$, and np is the number of measurement points. $[\mathrm{S}]$ can be calculated through global FE analysis [35] or substructuring approach [36].

Equation (1) is equivalent to a standard sparse recovery problem [15],

$$\{y\} = [X]\{\theta\} + \{\varepsilon\} \tag{5}$$

where $\{y\} \in R^M$ denotes the available measurements, $\{\theta\} \in R^N$ refers to the sparse parameters to be reconstructed, $[X] \in R^{M \times N}$ $(M < N)$ is referred to as the sensing matrix, and $\{\varepsilon\}$ is the error associated with the measurement noise. According to

sparse recovery theory, $\{\theta\}$ can be recovered by solving the following optimization programme [14]:

$$\hat{\theta} = \arg\min_{\hat{\theta}} \|[X]\{\theta\} - \{y\}\|_2^2 + \beta\|\{\theta\}\|_1 \quad (6)$$

As shown in Equation (5), through operating on the unknown vector $\{\theta\}$, the sensing matrix $[X]$ stores the information about $\{\theta\}$ in the measurements $\{y\}$. The performance of sparse recovery strongly relies on the properties of the sensing matrix. The measurements should retain as much information as possible to recover the unknown vector accurately using few measurements. Therefore, the sensing matrix which is used to sense the unknown parameters should be constructed with the columns as independently as possible.

Well-known criteria about the sensing matrix have been developed for exact recovery of sparse parameters on the basis of spark [37, 38], RIP [16] and mutual coherence [39, 40]. These conditions measure the independence of the columns of the sensing matrix and are closely related to one another. The spark of a given matrix is the smallest number of its linearly dependent columns [36]. The spark can only be obtained through a combinatorial search and thus is not convenient for implementation. The RIP was firstly proposed by Candès and Tao [16], based on which weaker recovery guarantees have been developed [41, 42]. The RIP constant of a matrix is difficult to be computed; consequently, the corresponding properties are difficult to verify.

The mutual coherence of the $M \times N$ sensing matrix $[X]$ is defined as [39]

$$\mu([X]) = \max \frac{|x_i^T x_j|}{\|x_i\| \cdot \|x_j\|}, \quad i, j = 1, \ldots, N \quad (7)$$

where x_i $(i = 1, \ldots, N)$ is the ith column of $[X]$. $\mu([X])$ measures the maximum linear dependency of the columns of matrix $[X]$. In this study, mutual coherence is used as the measure of the independence of the sensing matrix. According to Equations (1) and (5), the sensitivity matrix [S] defined in Equations (2)–(4) functions

as the sensing matrix. Sensor placement exerts an influence on mode shapes only, not on natural frequencies. Therefore, this study aims to determine an OSP so that the mutual coherence of the sensitivity matrix of the mode shapes, i.e. $\mu([S_\phi])$, is minimized.

Once the OSP is determined, or the measurement points are selected, the mode shape sensitivity that corresponds to the points will be included in the sensitivity matrix $[S_\phi]$. According to Equation (6), the corresponding model updating process aims to obtain the structural parameter through solving the following optimization problem:

$$\hat{p} = \arg\min_{\hat{p}}(\|\{R(p)\} - \{R^E\}\|_2^2 + \beta\|\{p\}\|_1) \tag{8}$$

where $\{R(p)\} = [S]\{p\} + \{R^0\}$ denotes the analytical modal parameters, and $\beta > 0$ is the regularization parameter. Natural frequencies and mode shapes are used during the process; therefore, Equation (8) can be expanded as [13]

$$\hat{p} = \arg\min_{\hat{p}}\left(\frac{1}{m}\sum_{i=1}^{m}\left[\frac{{\lambda_i}^A(\{p\}) - {\lambda_i}^E}{{\lambda_i}^E}\right]^2 + \frac{1}{m \times np}\sum_{i=1}^{m}\sum_{j=1}^{np}\left[{\phi_{ji}}^A(\{p\}) - {\phi_{ji}}^E\right]^2 + \frac{\beta}{n}\|\{p\}\|_1\right) \tag{9}$$

where superscripts '*A*' and '*E*' represent the analytical and experiment data, respectively. In the above equation, the eigenvalue residue, mode shape residue and solution norm are divided by their vector length for normalization purpose. This optimization problem can be solved using the active set or conjugate gradient algorithms [43]. The sensing matrix is calculated from the analytical model, and it is thus independent on the damage states.

3. Sensor Location Optimization using GA

As aforementioned, the selection of sensor locations is directly associated with the constitution of the sensitivity matrix and then affects the damage identification. An

OSP that results in the minimum mutual coherence of $[S_\phi]$ needs to be determined. Although the OSP problem has been investigated extensively over the past decades, it is challenging because it is basically a combinatorial problem. For example, we need to identify *np* distinct locations from all possible candidates.

Inspired by the Darwinian principle of natural selection, GA was firstly introduced by Holland [44] and has been proven to be a powerful tool in solving combinatorial optimization problems. In this study, a binary-coded GA is used to explore the OSP. A detailed description of GAs can be found in Goldberg [31] and Holland [44].

GA is a global optimization method that starts with an initial population of randomly generated chromosomes. Each chromosome refers to a candidate solution, and the component of a chromosome is called gene which is an integer of 0 or 1.

Considering the sensor placement problem, *np* sensors are to be placed amongst *l* candidate locations. One sensor placement is represented by one chromosome. Therefore, each chromosome consists of *l* genes which are set to 1 if a sensor is placed at the corresponding location or 0 otherwise. The total number of 1 in the chromosome is equal to *np*, the number of sensors. For example, the chromosome 1001000010 represents that three sensors are placed at positions 1, 4 and 9, amongst 10 candidate points.

Reproduction, crossover and mutation are three important genetic operators to produce a new offspring generation. The reproduction is conducted according to the fitness of the individual chromosome which is evaluated by an objective function. The chromosome with a high fitness has a high probability to be selected as the parent chromosome.

Once the parent chromosomes have been selected, they are paired up randomly for

mating, which is referred to as crossover. A crossover point along the chromosome pair is randomly assigned, then the substrings after the selected point are swapped to form two offspring. This process ensures that the features of two parent chromosomes are transferred to the next generation. A crossover probability p_c is applied to all parent chromosomes. p_c is generally close to 1 such that most parents will exchange their genes.

The operations of reproduction and crossover may reduce the population diversity, and thus the chromosomes tend to become significantly similar over several generations. Therefore, perturbations are introduced into the population to protect against the premature convergence to a non-optimal solution. Mutation serves the function by replacing a gene in a chromosome at a randomly selected location with a probability p_m. The mutation probability is usually a small value.

The processes of reproduction, crossover and mutation will repeat for many generations until a preset convergence criterion is satisfied. In the present OSP problem, the number of sensors is fixed. If the number of genes 1 in a chromosome is not np, then a forced mutation operator is introduced by replacing the number of genes 1 with 0 or the other way round. The forced mutation operator will not influence the GA convergence. Population size, p_c and p_m affect the GA performance and should be tuned in advance. The GA procedure is briefly shown in Figure 1.

A GA generally tends to maximize fitness, and the present OSP aims to minimize mutual coherence; hence, the minimization problem should be converted into a maximization problem. The concerned mutual coherence ranges between 0 and 1. The fitness function is thus defined as

$$f = 1 - \mu\left(\left[S_\phi\right]\right) \tag{10}$$

The fitness function operates on the encoded genes that measure the performance of a

specific sensor configuration. A sensor configuration with small mutual coherence has high fitness, then has a high probability to survive. The OSP corresponds to the minimum mutual coherence, thereby containing the most information about structural parameters and leading to the most accurate and reliable damage identification results. Two laboratory-tested examples are used to examine the feasibility and effectiveness of the proposed method.

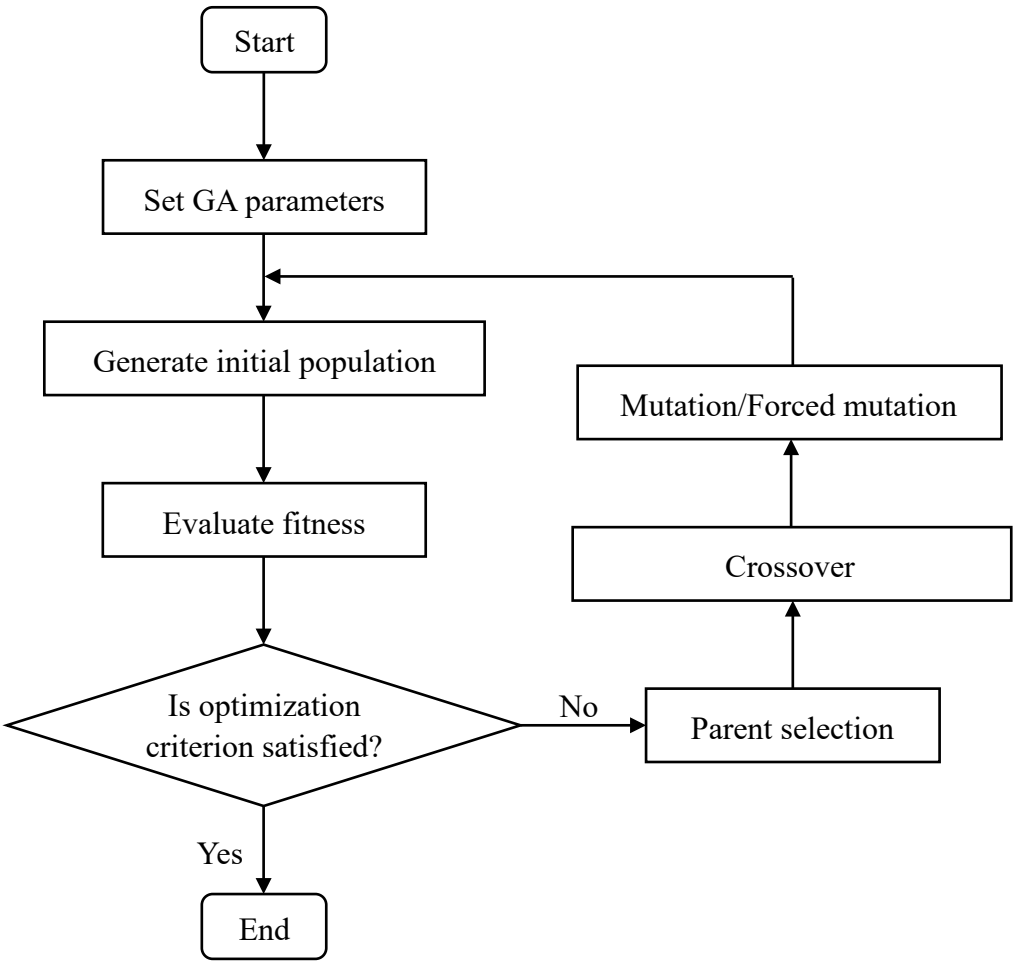

Figure 1 Flow chart of the GA

4. Example 1: A Cantilever Beam

4.1 Model descriptions

The experimental cantilever beam used here was initially reported by Hou *et al.* [45], as shown in Figure 2. The structural properties are listed in Table 1. Four damage scenarios (DSs) were introduced by three saw cuts, each with 10 mm length (Figure 2). In DS1, cut 1 has a depth of d = 10 mm. The depth of cut 1 was then increased to d = 15 mm in DS2. Subsequently, cuts 2 and 3 were introduced in DS3 and DS4, respectively. Cuts 2 and 3 have depths of d = 15 and 20 mm, respectively.

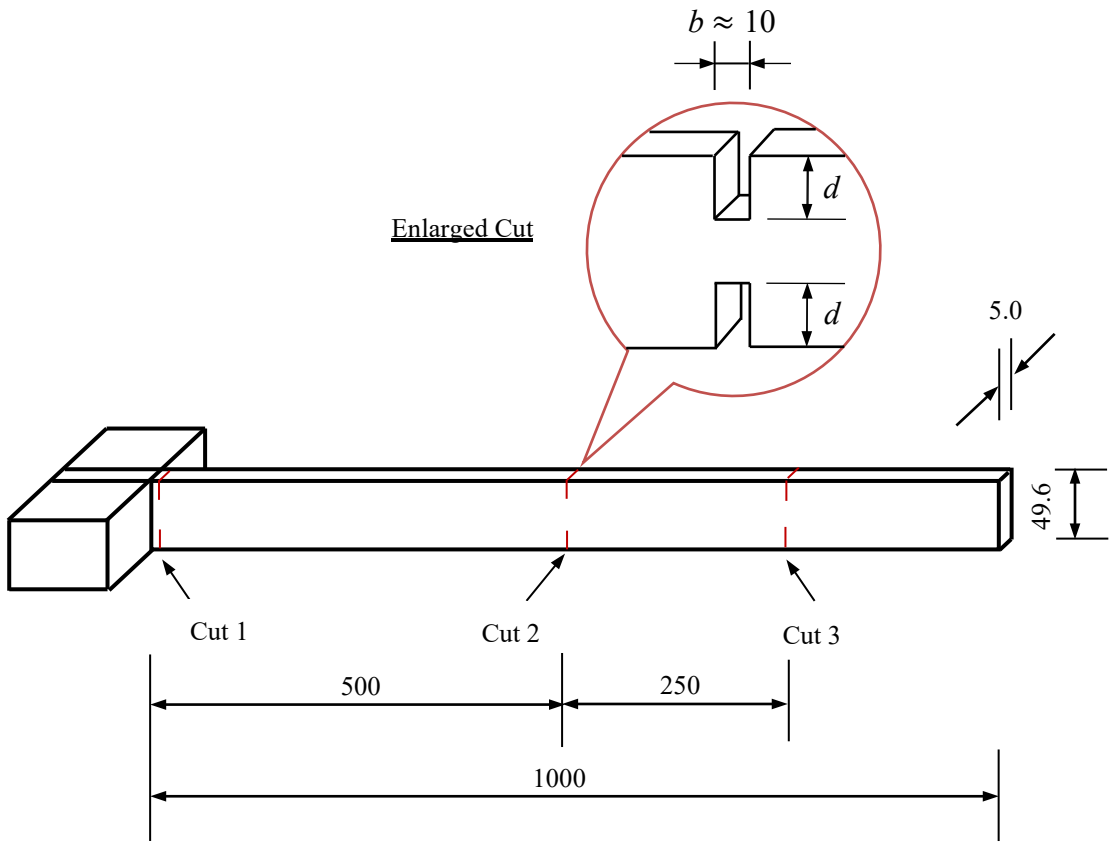

Figure 2 Overview of the beam structure (unit: mm)

Table 1 Structural properties of the beam

Properties	Value
Length L(mm)	1000
Cross-Sectional Area $A(\mathrm{mm}^2)$	49.6×5.0
Density $\rho(\mathrm{kg/m}^3)$	7.67×10^3
Young's Modulus $E(\mathrm{N/m}^2)$	2.0×10^{11}

A series of modal testing was conducted on the beam before and after damage. Ten accelerometers were equidistantly mounted on the beam (points 1–10 in Figure 3). The first six frequencies in the range of 0 Hz to 300 Hz and the associated mode shapes are extracted in all DSs, as listed in Table 2.

For the FE analysis, the beam is divided into 100 Euler–Bernoulli beam elements (Figure 3), each with 10 mm length which is identical to the length of the cuts. Therefore, the damage severity of each cut equals to the reduction in the moment of inertia of the cross section, which is quantified by the stiffness reduction factor (SRF). The actual damage locations and severities (SRF) for DS1 to DS4 are listed in Table 3.

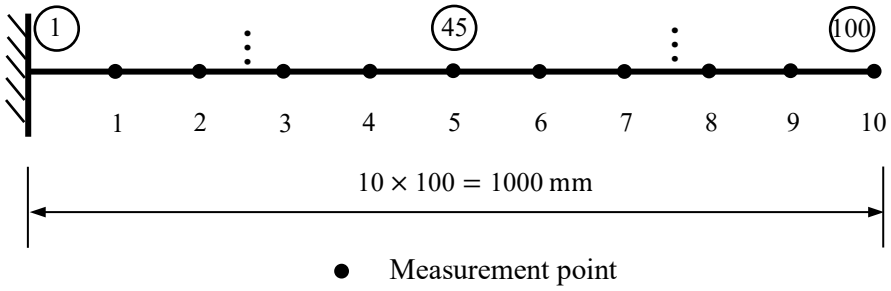

Figure 3 FE model and measurement configuration of the beam structure

Table 2 Modal data of the beam in the undamaged and damaged states

Mode no.	Undamaged	DS1		DS2		DS3		DS4	
	Freq. (Hz)	Freq. (Hz)	MAC	Freq. (Hz)	MAC	Freq. (Hz)	MAC	Freq. (Hz)	MAC
1	3.53	3.49 (−1.24)	99.99	3.38 (−4.41)	99.97	3.33 (−5.91)	99.98	3.36 (−4.91)	99.99
2	21.77	21.39 (−1.72)	99.95	20.85 (−4.26)	99.84	20.29 (−6.81)	99.86	19.76 (−9.22)	99.95
3	60.78	59.46 (−2.16)	99.88	58.93 (−3.04)	99.83	58.38 (−3.95)	99.57	54.37 (−10.55)	99.60
4	119.46	118.31 (−0.96)	99.88	116.01 (−2.88)	99.51	113.35 (−5.12)	99.23	106.31 (−11.01)	99.06
5	194.78	191.98 (−1.44)	99.78	188.74 (−3.10)	99.17	188.46 (−3.25)	98.87	187.17 (−3.91)	99.14
6	292.82	281.56 (−3.84)	98.07	286.76 (−2.07)	94.95	275.08 (−6.06)	98.26	267.45 (−8.66)	97.26
Average		(−1.90)	99.59	(−3.29)	98.88	(−5.18)	99.30	(−8.04)	99.17

Note: Values in parentheses are the frequency change ratios (%) between the damaged and undamaged states.

Table 3 Damage locations and severities for four DSs of the beam

Scenario	DS1	DS2	DS3	DS4
Damage location and severity	SRF(1) = –40%	SRF(1) = –60%	SRF(1) = –60% SRF(50) = –60%	SRF(1) = –60% SRF(50) = –60% SRF(75) = –80%

4.2 OSP using GA

Although 10 sensors have been placed on the beam (i.e. Nos. 1–10 in Figure 3), we select 5 points out of 10 to demonstrate the proposed OSP technique. Equation (10) is then maximised, and the maximum fitness corresponds to OSP. In the binary-coded GA, the population size is set to 100. The probabilities of crossover and mutation, i.e. p_c and p_m, are 0.85 and 0.1, respectively. The number of generations is 100.

The initial population in GA is randomly generated and may affect the converged results; therefore, the presented GA runs 10 times to investigate the convergence and repeatability of the proposed sensor placement technique. The results show that the obtained sensor locations in 10 operations are identical, i.e. points 4, 6, 8, 9 and 10, as shown in Figure 4. The selected sensor locations are close to the free end of the cantilever beam. The numbers of generations upon convergence during the 10 runs are listed in Table 4. All runs converge within 10 generations, thus indicating the fast convergence of the present technique.

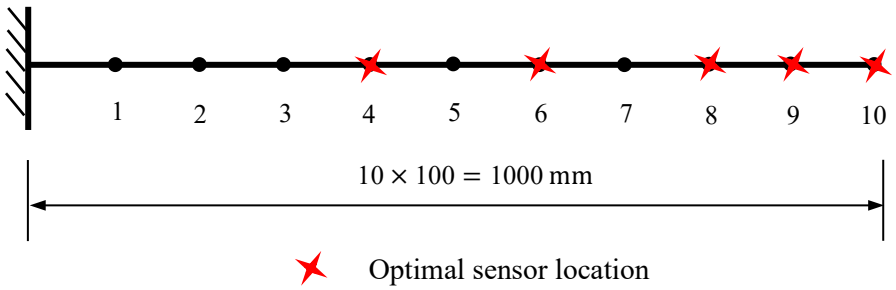

Figure 4 OSP of the beam structure

Table 4 Convergence of different initial populations

Run no.	1	2	3	4	5	6	7	8	9	10
Number of generations	9	8	7	8	6	8	8	8	9	5

The maximal and averaged fitness with respect to the generation history during one operation are shown in Figure 5. Both increase with the generation number. The maximum value tends to a constant rapidly, and the averaged fitness reaches the maximum after nine generations.

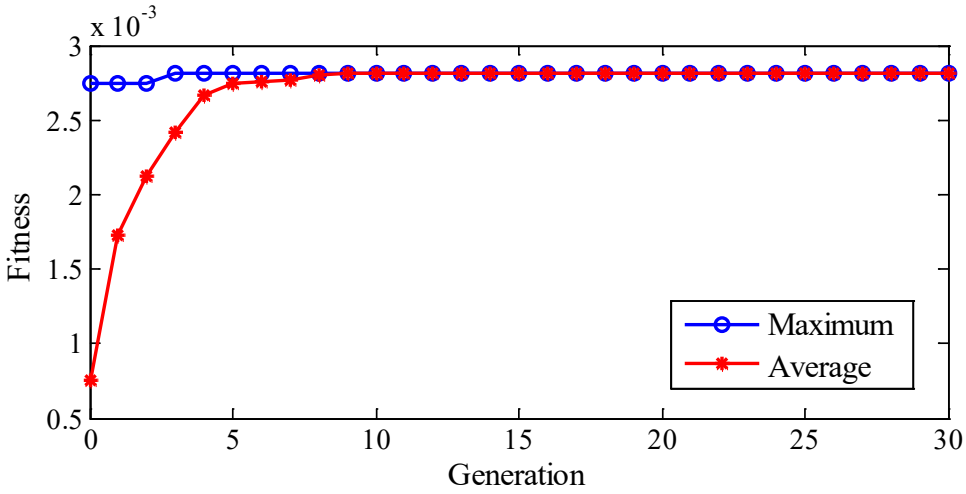

Figure 5 History of convergence for the OSP of the beam

4.3 Damage detection results

Damage detection is conducted using the selected sensor subset to demonstrate the effectiveness of the proposed OSP technique. The first six frequencies and the mode shapes that correspond to the five selected points are used in Equation (9). The residual and solution norms are utilized to determine the appropriate regularization parameter [45]. The parameter which keeps both norms small is determined as an appropriate regularization parameter. The damage identification results of the four DSs are shown in Figure 6 together with the corresponding regularization parameters. The actual damage locations are detected successfully for all DSs. For DS1 and DS2, the identified damage severities are slightly larger than the true values, i.e. 40% and 60% reduction, respectively. For DS3, the damage at the mid-span is quantified accurately, but the severity of the damaged element no. 1 is still larger than the true value. For DS4, the damaged elements (nos. 1, 45 and 75) are quantified with good accuracy. Although several elements are falsely identified as damaged, their SRF values are very small (less than 5%) and the errors can be ignored. Therefore, all DSs are correctly identified using the mode shapes that correspond to the proposed OSP. The present damage identification results are similar to those using 10 sensors conducted by Hou *et al*. [45].

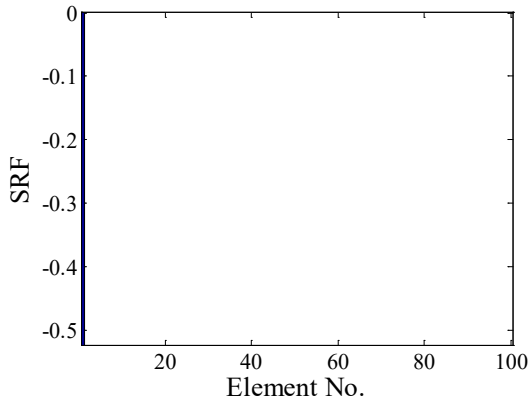

(a) DS1 ($\beta = 0.10$)

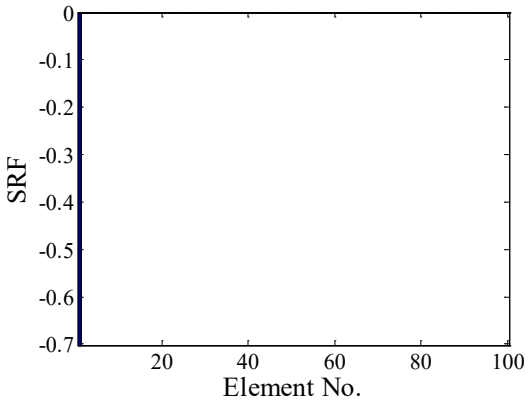

(b) DS2 ($\beta = 0.20$)

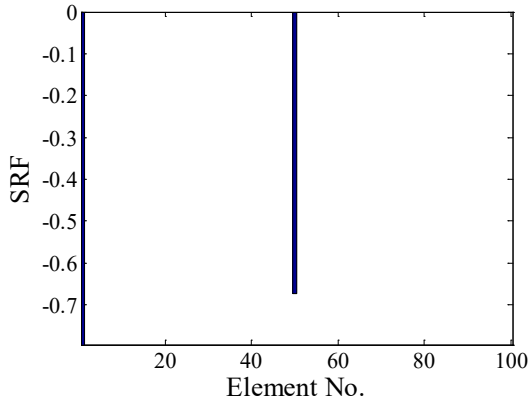

(c) DS3 ($\beta = 0.08$)

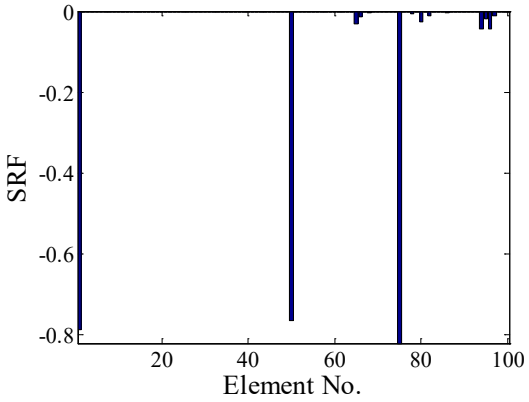

(d) DS4 ($\beta = 0.12$)

Figure 6 Damage identification results for four DSs of the beam

The beam model has 100 elements and thus has 100 SRF values to be identified. However, only the first six frequencies and the mode shapes at five measurement points are available, i.e. 36 measurement data can be used. Damage identification is an extremely underdetermined problem. The l_1 regularisation technique detects all damaged elements accurately in all four scenarios.

5. Example 2: A Three-storey Frame

5.1 Model descriptions

Another example is a three-storey steel frame which was tested by Hou *et al*. [13], as shown in Figure 7. The mass density of the frame is 7.92×10^3 kg/m^3, and the Young's modulus is estimated as 2.0×10^{11} N/m^2. Two saw cuts were introduced into the frame model in sequence, which corresponds to two DSs (Figure 7). Cut 1 is at the bottom of the column, and cut 2 is located at the beam-column joint. The saw cuts have the same length b = 20 mm and depth d = 22.5 mm. The moments of inertia of the cut sections are thus reduced by 60%.

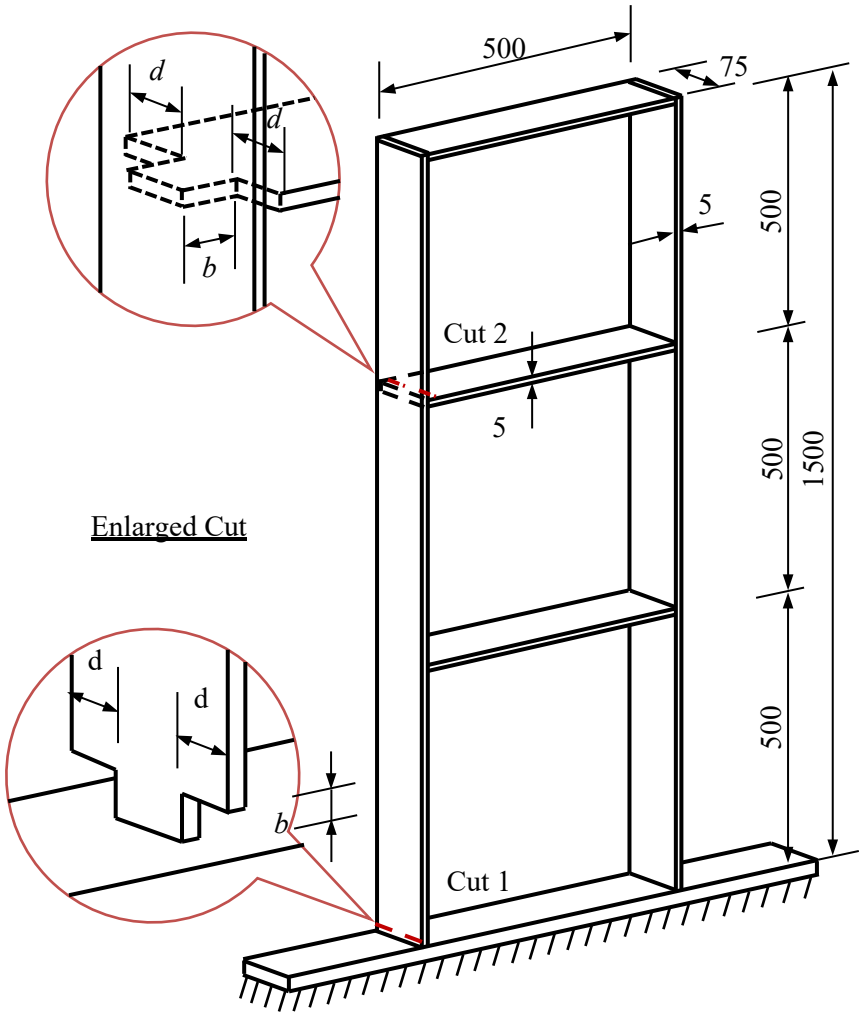

Figure 7 Configuration of the frame (Unit: mm)

The modal testing was conducted on the intact frame and damaged ones. The accelerations at 39 points, as shown in Figure 8, were measured during the laboratory test. For the beams and columns, the vertical and horizontal accelerations were measured, respectively. The first eight frequencies and mode shapes were extracted and used for damage detection. The modal data of the frame in different states are listed in Table 6.

In the FE analysis, the frame is modelled with 225 elements, and each are 20 mm long, which is identical to that of the cuts. Cuts 1 and 2 are located at elements 1 and 176, respectively. Therefore, SRF(1) = –60% in DS1, and SRF(1) = SRF(176) = –60%

in DS2.

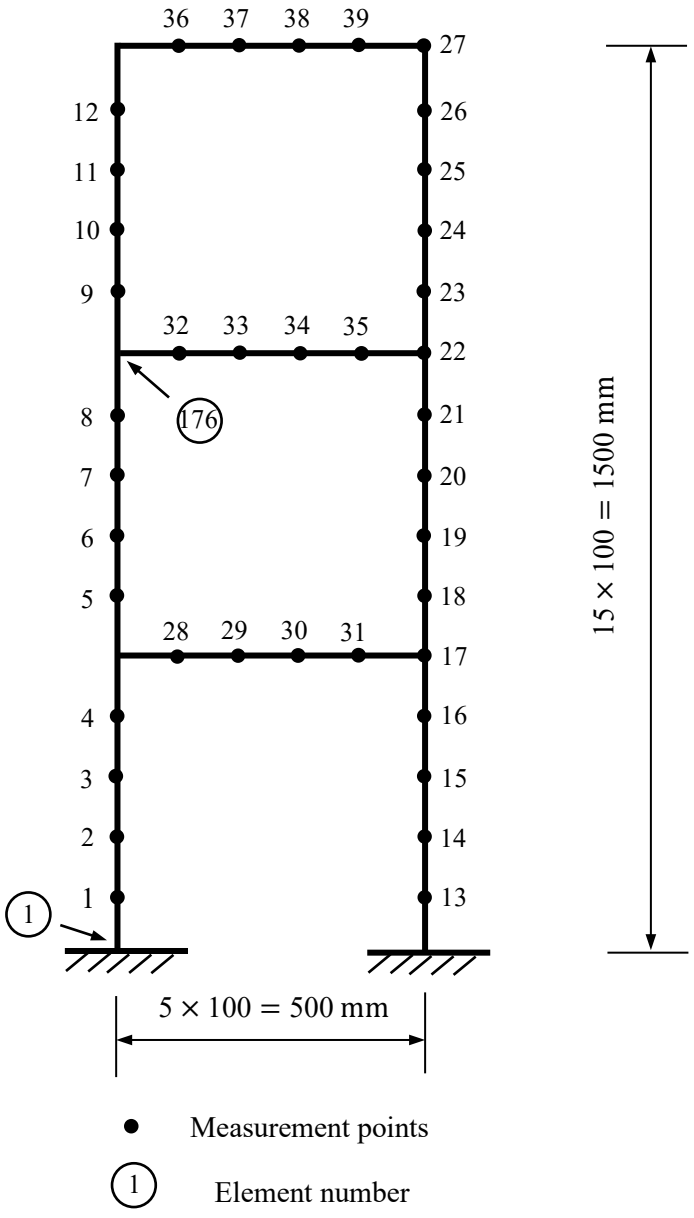

Figure 8 FE model and measurement configuration of the frame

Table 6 Modal data of the undamaged and damaged frame structures

Mode	Undamaged	DS1		DS2	
no.	Freq. (Hz)	Freq. (Hz)	MAC	Freq. (Hz)	MAC
1	4.23	4.13 (–2.31)	92.02	4.08 (–3.53)	95.78
2	14.03	13.75 (–1.96)	99.02	13.45 (–4.11)	97.49
3	25.45	25.14 (–1.19)	98.87	25.13 (–1.23)	99.01
4	44.81	44.70 (–0.23)	94.74	44.69 (–0.27)	97.59
5	58.12	57.39 (–1.24)	92.45	57.28 (–1.44)	91.46
6	68.36	67.34 (–1.49)	93.01	66.11 (–3.29)	88.14
7	72.27	72.06 (–0.28)	96.30	71.42 (–1.18)	85.80
8	91.73	89.14 (–2.83)	86.79	88.51 (–3.52)	76.38
Average		(–1.44)	94.15	(–2.32)	91.46

Note: Values in parentheses are the frequency change ratios (%) between the damaged and undamaged states.

5.2 OSP using GA

The proposed sensor placement technique is applied to determine the sensor locations for the frame. The population size is set to 200. The crossover and mutation probabilities, i.e. p_c and p_m, are set to 0.85 and 0.1, respectively. The number of generations is 150.

As introduced previously, the frame has 39 candidate locations in total. Two measurement selection schemes are studied to investigate the effect of the number of sensors. Scheme 1 has 20 points, and scheme 2 has 15 points. Using the proposed algorithm, the selected measurement points for the two schemes are shown in Figure 9. Although the two different measurement schemes are determined independently, the selected sensor locations in scheme 2 are from those of scheme 1.

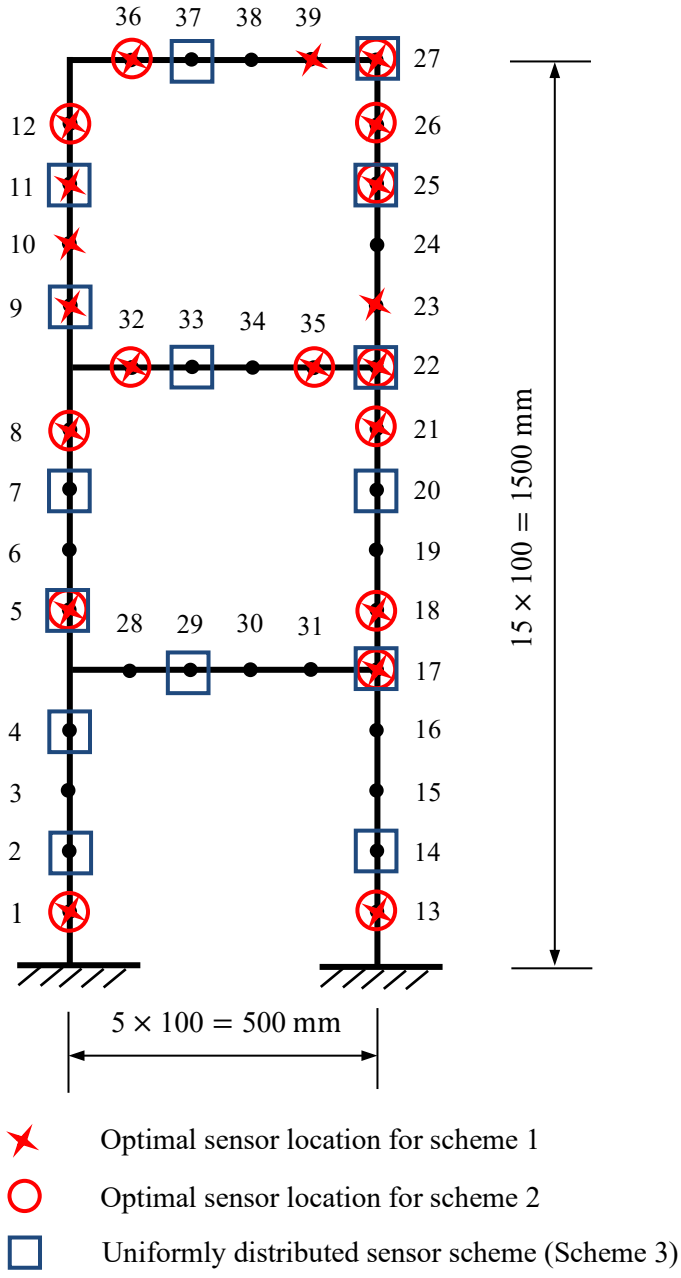

Figure 9 OSP of the frame

The fitness convergence curves for two schemes are shown in Figure 10. The maximum and average fitness values steadily tend to a constant with the increase in the generation number. When 20 points are required (Scheme 1), the average fitness reaches the maximum fitness value of 3.34×10^{-3} in 52 generations. When 15 points are selected (Scheme 2), the average fitness reaches the maximum fitness

value of 3.23×10^{-3} in 62 generations.

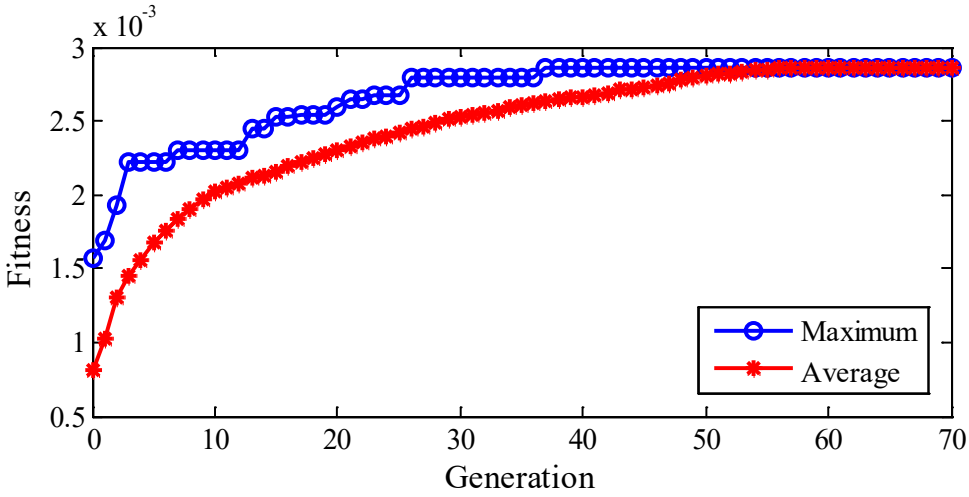

(a) Scheme 1: 20 measurement points

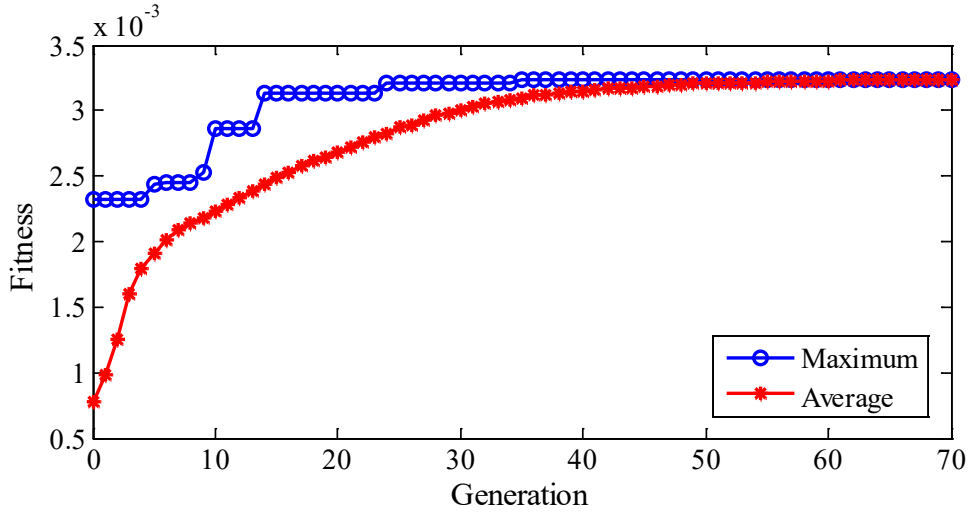

(b) Scheme 2: 15 measurement points

Figure 10 History of convergence for OSP of the frame

In schemes 1 and 2, the proposed GA is run for 10 times with different initial populations. The number of generations upon convergence is listed in Table 7. In the case of 20 measurement points, all 10 runs converge within 63 generations. In the other case of 15 measurement points, all 10 runs converge in 92 generations. In each scheme, 10 runs result in the same OSP. This result shows that the proposed GA

based on mutual coherence is robust, and the OSP obtained is reliable.

Table 7 Convergence for different numbers of measurement points

Run no.	Number of generations	
	Scheme 1 (20 measurement points)	Scheme 2 (15 measurement points)
1	58	62
2	42	63
3	45	84
4	63	68
5	62	63
6	56	92
7	63	64
8	57	80
9	50	60
10	63	70

5.3 Damage detection results

Damage detection of the frame is conducted using the measured frequencies and mode shapes that correspond to the selected sensor locations. The SRF vector is extremely sparse because only 1 or 2 elements are damaged amongst the total 225 elements. For measurement schemes 1 and 2, 168 and 128 measurement data are respectively available; both lead to an underdetermined problem. For comparison, the proposed l_1-regularized damage detection technique is also applied to measurement scheme 3 which also contains 15 measurement points as scheme 2. Its sensor locations are uniformly selected in a conventional manner (Figure 9).

The damage identification results of the three schemes for two DSs are shown in Figure 11. For DS1, the damage location and severity (SRF(1)= −0.6) can be

identified accurately using all three schemes. For DS2, two damaged elements (nos. 1 and 176) are located accurately, and no false identification occurs when schemes 1 and 2 are used, although the identified damage severity has a small error. The numbers of measurement points for schemes 2 and 3 are identical. However, the damage identification results for DS2 are different. For scheme 3, the damaged element no. 1 is detected successfully, but the element no. 166 is not. Results show that sensor placement exerts a significant effect on damage detection accuracy and that damage can be accurately identified on the basis of the proposed OSP technique.

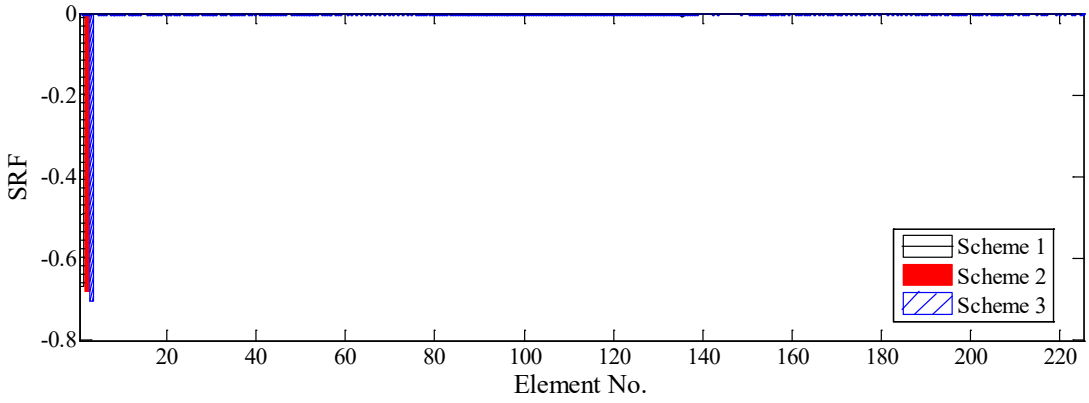

(a) DS1

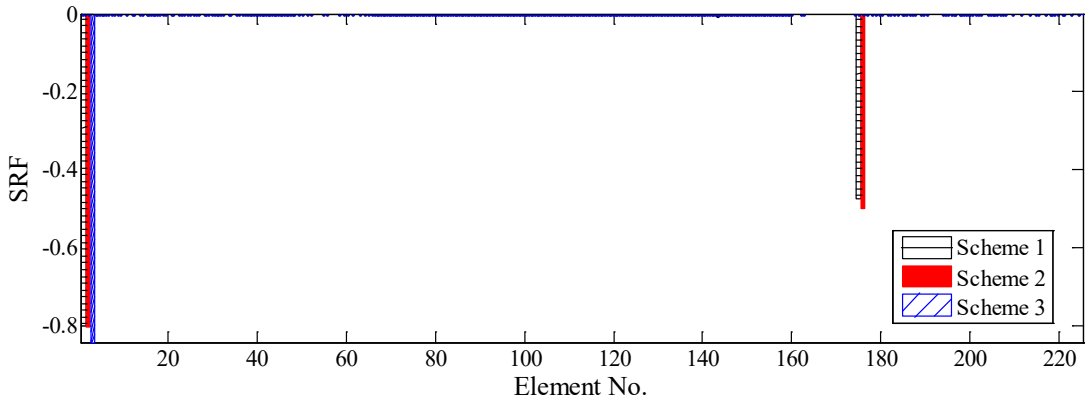

(b) DS2

Figure 11 Damage identification results of the frame using different measurement points

6. Conclusions and discussion

Sensor locations play an important role in damage identification and selection of sensor locations is a combinatorial problem. A GA-based sensor placement technique is proposed in this study for minimizing the mutual coherence of the sensitivity matrix in l_1-regularized damage detection. The present technique works on the sensitivity matrix in the undamaged state and thus does not need the prior knowledge of damage location and severity. Therefore it is applicable to damage detection of real structures.

Although GAs usually depend on the initial population, the experimental studies demonstrate that the present GA offers consistent OSP results using different initial populations. Two examples also show that satisfactory damage detection results are obtained using the modal data based on the optimal sensor configuration. Moreover, the l_1 regularization technique is effective in identifying sparse damage accurately.

Acknowledgements

This research was supported by the PolyU Research Grant (Project No. 1-BBAG), RGC General Research Grant (Project No. PolyU 152125/17E) and the National Natural Science Foundation of China (Project No. 51678364).

References

1. Kim JT, Stubbs N. Crack detection in beam-type structures using frequency data. *Journal of Sound and Vibration* 2003; **259**(1):145–160.

2. Shi ZY, Law SS, Zhang LM. Damage localization by directly using incomplete mode shapes. *Journal of Engineering Mechanics* 2000; **126**(6):656–660.

3. Xu YL, Zhang J, Li JC, Xia Y. Experimental Investigation on Statistical Moment-based Structural Damage Detection Method. *Structural Health Monitoring* 2009; **8**(6):555–571.

4. Salawu OS. Detection of structural damage through changes in frequency: a review. *Engineering Structures* 1997; **19**(9):718–723.

5. Doebling SW, Farrar CR, Prime MB, Shevitz DW. Damage identification and health monitoring of structural and mechanical systems from changes in their vibration characteristics: a literature review, *Los Alamos National Laboratory Report*, 1996.

6. Sohn H, Farrar CR, Hemez FM, Shunk DD, Stinemates DW, Nadler BR, Czarnecki JJ. A review of structural health monitoring literature: 1996–2001, *Los Alamos National Laboratory Report*, 2003.

7. Engl HW, Hanke M, Neubauer A. *Regularization of Inverse Problems*. Kluwer Academic Publishers Group, Dordrecht, The Netherlands, 1996.

8. Bao Y, Li H, Ou J. Emerging data technology in structural health monitoring: compressive sensing technology. *Journal of Civil Structural Health Monitoring* 2014; **2**(4):77–90.

9. Yang Y, Nagarajaiah S. Structural damage identification via a combination of blind feature extraction and sparse representation classification. *Mechanical Systems and Signal Processing* 2014; **45**(1):1–23.

10. Hernandez EM. Identification of isolated structural damage from incomplete spectrum information using l_1-norm minimization. *Mechanical Systems and Signal Processing* 2014; **46**(1):59–69.

11. Zhou XQ, Xia Y, Weng S. L_1 regularization approach to structural damage detection using frequency data. *Structural Health Monitoring* 2015; **14**(6):571–582.

12. Zhang C, Xu Y. Comparative studies on damage identification with Tikhonov regularization and sparse regularization. *Structural Control and Health Monitoring* 2016; **23**(3):560–579.

13. Hou RR, Xia Y, Zhou XQ. Structural damage detection based on l_1 regularization using natural frequencies and mode shapes. *Structural Control and Health Monitoring* 2018; **25**(3), e2107.

14. Candès EJ. Compressive sampling. *Proceedings of the International Congress of Mathematicians*, Madrid, Spain, 2006; 1433–1452.

15. Theodoridis S, Kopsinis Y, Slavakis K. Sparsity-aware learning and compressed sensing: An overview. *Acadamic Press Library in Singnal Processing* 2013; 1271–1377.

16. Candès EJ, Tao T. Decoding by linear programming. *IEEE Transactions on Information Theory* 2005; **51**(12):4203–4215.

17. Candès EJ, Romberg J, Tao T. Robust uncertainty principles: exact signal reconstruction from highly incomplete frequency information. *IEEE Transactions on Information Theory* 2006; 5:489–509.

18. Kammer DC. Sensor placement for on-orbit modal identification and correlation of large space structures. *Journal of Guidance, Control Dynamics* 1991; **14**(2):251–259

19. Kirkegaard PH, Brincker R. On the optimal locations of sensors for parametric identification of linear structural systems, *Mechanical Systems and Signal Processing* 1994; 8:639–647.

20. Papadimitriou C. Optimal sensor placement methodology for parametric identification of structural systems. *Journal of Sound and Vibration* 2004; 278:923–947.

21. Chang M, Pakzad SN. Optimal Sensor Placement for Structural Modal Identification. *Journal of Bridge Engineering*, *ASCE*, 2014; **19**(6):04014019–1.

22. Heo G, Wang ML, Satpathi D. Optimal transducer placement for health monitoring of long span bridge. *Soil Dynamics and Earthquake Engineering* 1997; 16:495–502.

23. Meo M, Zumpano G. On the optimal sensor placement techniques for a bridge structure. *Engineering Structures* 2005; **27**(10):1488–1497.

24. Yi TH, Li HN, Zhang XD. Health monitoring sensor placement optimization for Canton Tower using immune monkey algorithm. *Structural Control and Health Monitoring* 2015; **22**(1):123–138.

25. Hemez FM, Farhat C. An energy based optimum sensor placement criterion and its application to structural damage detection. *Proceedings of 12th International Modal Analysis Conference (IMAC)*, Society of Experimental Mechanics, Honolulu, 1994; 1568–1575.

26. Zhou XQ, Xia Y, Hao H. Sensor placement for structural damage detection considering the measurement uncertainties. *Advances in Structural Engineering* 2013; 16(5):899–907.

27. Shi ZY, Law SS, Zhang LM. Optimum sensor placement for structural damage detection. *Journal of Engineering Mechanics, ASCE*, 2000; **126**(11):1173–1179.

28. Xia Y, Hao H. Measurement selection for vibration-based structural damage identification. *Journal of Sound and vibration* 2000; **236**(1): 89–104.

29. Casciati S. Stiffness identification and damage localization via differential evolution algorithms. *Structural Control and Health Monitoring* 2008; 15:436–449.

30. Casciati S, Elia L. Damage localization in a cable-stayed bridge via bio-inspired metaheuristic tools. *Structural Control and Health Monitoring* 2017; 24, e1922.

31. Goldberg DE. Genetic algorithms in search, machine learning and optimisation. New York, Addison Wesley, 1989.

32. Yao L, Sethares WA, Kammer DC. Sensor placement for on-orbit modal identification via a genetic algorithm. *AIAA Journal* 1993; 31:1167–9.

33. Worden K, Burrows AP. Optimal sensor placement for fault detection. *Engineering Structures* 2001; **23**(8):885–901.

34. Liu W, Gao WC, Sun YI, Xu MJ. Optimal sensor placement for spatial lattice structure based on genetic algorithms. *Journal of Sound and Vibration* 2008; 317:175–189.

35. Nelson RB. Simplified calculation of eigenvector derivatives. *AIAA Journal* 1976; **14**(9):1201–1205.

36. Weng S, Xia Y, Xu YL, Zhu HP. An iterative substructuring approach to the

calculation of eigensolution and eigensensitivity. *Journal of Sound and Vibration* 2011; **330**(14):3368–3380.

37. Gorodnitsky IF, Rao BD. Sparse signal reconstruction from limited data using FOCUSS: A reweighted minimum norm algorithm. *IEEE Transactions on Signal Processing* 1997; **45**(3):600–616.

38. Donoho DL, Elad M. Optimally sparse representation in general (nonorthogonal) dictionaries via l_1 minimization. *Proceedings of the National Academy Sciences* 2003; 100:2197–2202.

39. Mallat S, Zhang Z. Matching pursuit in a time-frequency dictionary. *IEEE Transactions on Signal Processing* 1993; **49**(12):3397–3415.

40. Elad M. Optimized projections for compressed sensing. *IEEE Transactions on Signal Processing* 2007; **55**(12):5695–5702.

41. Mo Q, Li S. New bounds on the restricted isometry constant δ_{2k}. *Applied Computational Harmonic Analysis* 2011; **31**(3):460–468.

42. Foucart S. A note on guaranteed sparse recovery via l_1-minimization. *Applied and Computational Harmonic Analysis* 2010; **29**(1):97–103.

43. Boyd S, Vandanberghe L. *Convex Optimization*. Cambridge University Press: New York, NY, 2004.

44. Holland JH. *Adaption in natural and artificial systems*. Ann Arbor: University of Michigan Press, 1975.

45. Hou RR, Xia Y, Bao YQ, Zhou XQ. Selection of regularization parameter for l_1-regularized damage detection. *Journal of Sound and Vibration* 2018; 423:141–160.